

PHYSICS

Direct light-induced spin transfer between different elements in a spintronic Heusler material via femtosecond laser excitation

Phoebe Tengdin^{1*}, Christian Gentry¹, Adam Blonsky¹, Dmitriy Zusin¹, Michael Gerrity¹, Lukas Hellbrück², Moritz Hofherr², Justin Shaw³, Yaroslav Kvashnin⁴, Erna K. Delczeg-Czirjak⁴, Monika Arora³, Hans Nembach^{1,3}, Tom J. Silva³, Stefan Mathias⁵, Martin Aeschlimann², Henry C. Kapteyn¹, Danny Thonig^{4,6}, Konstantinos Koumpouras⁷, Olle Eriksson^{4,6}, Margaret M. Murnane¹

Heusler compounds are exciting materials for future spintronics applications because they display a wide range of tunable electronic and magnetic interactions. Here, we use a femtosecond laser to directly transfer spin polarization from one element to another in a half-metallic Heusler material, Co_2MnGe . This spin transfer initiates as soon as light is incident on the material, demonstrating spatial transfer of angular momentum between neighboring atomic sites on time scales < 10 fs. Using ultrafast high harmonic pulses to simultaneously and independently probe the magnetic state of two elements during laser excitation, we find that the magnetization of Co is enhanced, while that of Mn rapidly quenches. Density functional theory calculations show that the optical excitation directly transfers spin from one magnetic sublattice to another through preferred spin-polarized excitation pathways. This direct manipulation of spins via light provides a path toward spintronic devices that can operate on few-femtosecond or faster time scales.

INTRODUCTION

Ultralow-power, high-performance nonvolatile memory and logic devices based on magnetic spin (“spintronics”) are starting to make inroads into conventional computing and represent prime candidates for practical quantum technologies. Half-metallic Heusler compounds are particularly promising candidates for efficiently generating pure spin currents for spintronics devices (1). This is due to their unique band structure (2–4), where one spin channel (the majority band) is metallic in nature, but the other spin channel (minority) is insulating, with a bandgap at the Fermi energy (see Fig. 1). However, fully exploiting the capabilities of new materials and technologies will require a detailed understanding of the magnetism at the nanoscale. At present, our understanding of spin interactions is crude and predominantly phenomenological, and experiments are constrained by a limited ability to directly observe and control spin interactions on all relevant time and length scales. While the fundamental length and time scales for magnetic phenomena are nanometers (exchange length) and femtoseconds (exchange splitting), tools that enable the exploration of dynamics at these scales have only recently become available.

For over two decades, ultrafast laser excitation has been used to quench or switch the magnetic state of materials (5–7). All-optical switching has been demonstrated experimentally using circularly

and linearly polarized light. However, the response of the material is not instantaneous but takes place on picosecond time scales—long after the laser excitation pulse (8), and in some cases also requires the cumulative effect of many pulses (9, 10). Similarly, laser-induced demagnetization of materials has almost exclusively been understood as a secondary process: triggered by an initial hot electron distribution followed by electron-phonon spin flip and other processes to absorb the spin angular momentum on ~ 0.5 -ps time scales (5). In the search for materials that enable fast spin manipulation, researchers have investigated several Heusler alloys using ultrafast femtosecond laser pulses to drive the system into a non-equilibrium state while monitoring the response of the system with magneto-optics (2, 3, 11, 12). However, visible lasers probe the net magnetization averaged over all elements in the material. Very recent theoretical papers exploring laser-excited Heusler compounds have suggested the possibility of light-induced spin transfer from one element to another on extremely fast (< 10 fs) time scales (13, 14). This could, in theory, enable the ultimate goal of ultrafast direct optical manipulation of the magnetic state of a material, provided these dynamics can be observed.

Ultrafast extreme ultraviolet (EUV) high harmonic pulses make it possible to uncover the element-specific spin dynamics in multi-component magnetic systems, providing rich new information not accessible using visible light. Recent work has explored ultrafast laser-induced spin dynamics in ferromagnetic alloys and multilayers, where distinct responses—such as the existence of a time lag between the quenching of the magnetization of different elements in an FeNi alloy—were observed (15). Other recent work has shown that an ultrafast laser pulse can create high-energy magnons in simple ferromagnets, on time scales 10 times faster than previously suspected, within tens of femtoseconds (16, 17).

Here, we show that a single ultrafast laser pulse can directly transfer spin polarization from one magnetic element to another in

¹Department of Physics and JILA, University of Colorado and NIST, Boulder, CO 80309, USA. ²Research Center OPTIMAS, University of Kaiserslautern, Erwin-Schroedinger Strasse 46, 67663 Kaiserslautern, Germany. ³Quantum Electromagnetics Division, National Institute of Standards and Technology, Boulder, CO 80305, USA. ⁴Department of Physics and Astronomy, University Uppsala, S-75120 Uppsala, Sweden. ⁵Georg-August-Universität Göttingen, I. Physikalisches Institut, Friedrich-Hund-Platz 1, 37077 Göttingen, Germany. ⁶School of Science and Technology, Örebro University, SE-701 82 Örebro, Sweden. ⁷Department of Engineering Sciences and Mathematics, Luleå University, SE-E186 Luleå, Sweden.

*Corresponding author. Email: phoebe.tengdin@colorado.edu

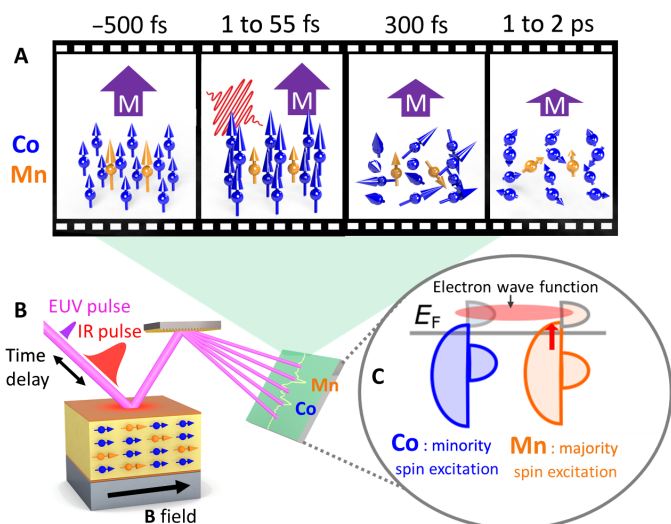


Fig. 1. Direct light-induced spin transfer in Co₂MnGe. (A) Representation of spin dynamics in Co₂MnGe. Before excitation, Mn atoms (orange arrows) have a 3× larger magnetic moment than Co atoms (blue arrows), which are 2× more abundant in the bcc lattice. The purple arrow represents the net magnetic moment of the compound. Immediately upon excitation by light (within a few femtoseconds), the Mn moment starts to decrease and the Co magnetic moment grows by 10%. Hundreds of femtoseconds later, the Mn and Co atomic spins become disordered, and the angular momentum begins to transfer to the lattice. After 1 to 2 ps, the spins have reached their maximum quenching. (B) Schematic of the experimental setup. Ultrafast femtosecond laser pulses excite the sample, while the element-specific magnetization dynamics are tracked using femtosecond EUV pulses. IR, infrared. (C) Density of states for each element in the half-metal. Note that the minority spin channel is gapped, with no available states at the Fermi level for the minority channel. Critically, this gap is larger for Mn than for Co. After excitation (dominated by transitions from the Mn majority states, marked by a red arrow), the conduction band states are hybridized, as illustrated by the shared red wave function.

the half-metal Heusler compound Co₂MnGe. This spin transfer initiates as soon as light is incident on the material—suggesting near-instantaneous femtosecond to attosecond time scales for this process. We use ~10 fs EUV high harmonic pulses resonant at the 3p edges of cobalt and manganese to measure the transverse magneto-optical Kerr effect (TMOKE) of each element simultaneously and independently. This allows us to observe a surprising disparity between the response of the two magnetic sublattices: The magnetization of cobalt is transiently enhanced over the entire laser pump pulse, while that of manganese quenches rapidly. Density functional theory (DFT) calculations (18, 19) show that optical excitations are more likely to occur from the majority spin channel of Mn into the shared states of the conduction band, which are primarily Co in character. This imbalance of allowed excitation pathways therefore induces a direct and instantaneous transfer of spin polarization from Mn sites to Co sites that occurs during the entire laser pulse. As a control, we probed the disordered non-half-metallic (A2) phase of the same material and observed no enhancement of magnetization or transfer of spin polarization. This is consistent with electronic structure theory that does not support any imbalance in the excited spin population of manganese in this phase. The enhancement of ferromagnetic ordering demonstrates direct manipulation of spins via light, thus providing a path toward spintronic logic devices such as switches that can operate on few-femtosecond or even faster time scales.

These results show that by tuning the band structure, we can control the ultrafast magnetic response in a quantum material.

We note that this new ability to directly manipulate the spin polarization in a material using light is different from all past experimental observations, where a cascaded sequence of events were assumed to lead to changes in the magnetization after electrons were excited by a femtosecond laser. These include phonon-mediated spin flip processes that requires ~100- to 500-fs time scales to efficiently change the magnetization, and which can only lead to a reduction in magnetization. Similarly, ultrafast high-energy magnon generation can also only lead to a reduction in magnetization. Super diffusive spin transport can lead to an enhancement in the magnetization in magnetic multilayers—due to laser-excited spin-polarized currents that arise from the different scattering lengths (times) for majority versus minority spins. However, our geometry does not support spin currents, and moreover, the signature of spin currents has always appeared on relatively long time scales, after the hot electron-spin system has cooled because of phonon-mediated and other spin flip scattering processes.

Figure 1A provides an overview of the ultrafast spin dynamics that occur in the half-metallic phase of Co₂MnGe. Before the pump pulse arrives, the material is ferromagnetically ordered, with a B2 structure (the CsCl structure), where Co occupies the corner sites and the body-centered position is randomly occupied by Mn or Ge. Note that the Mn atoms carry ~3× as much magnetic moment as the Co atoms. As shown in Figs. 1 and 2, within the time scale of the laser pump pulse, there is a near-instantaneous direct transfer of magnetization from the Mn atoms to the Co atoms: The magnetic moment of the Co atoms is enhanced, while the magnetization of the Mn atoms simultaneously decreases. After the pump pulse, the material continues to demagnetize, dissipating the angular momentum into the lattice within a picosecond. We emphasize that the initial magnetic response of the system is completely dominated by direct optical excitation, while rotation of atomic magnetic moments enters at a second stage. This is corroborated by a theoretical analysis based on the atomistic Landau-Lifshitz-Gilbert (aLLG) equation (20) (presented in the Supplementary Materials), which fails to describe the initial phase of the magnetic response (<250 fs) but provides the correct trend for longer time scales (>500 fs).

RESULTS

Figure 1B shows the experimental setup used to simultaneously measure the response of Co and Mn after ultrafast excitation. We excite the sample with an infrared laser pulse with a photon energy of 1.55 eV and 55-fs full width at half maximum (FWHM) in duration. To record the magnetic response, part of the laser light is directed into a He-filled hollow core waveguide to generate 10-fs high harmonic EUV pulses that are simultaneously resonant with the 3p edges of Co (59 eV) and Mn (47 eV). The EUV TMOKE signal is constructed by a differential asymmetry [A] measurement with $A = \frac{I_+ - I_-}{I_+ + I_-}$, where I_+ and I_- are the intensities of the EUV light that is reflected from the sample for opposite directions of magnetization. The responses from individual elements are separated via a spectrometer (21). A more detailed schematic of the experimental layout is given in the Supplementary Materials. See fig. S2A for an illustration of which harmonic energies are used to extract the Co and Mn signals independently.

Figure 2A plots the experimentally measured asymmetry of Co and Mn in the half-metallic B2 phase as a function of pump probe

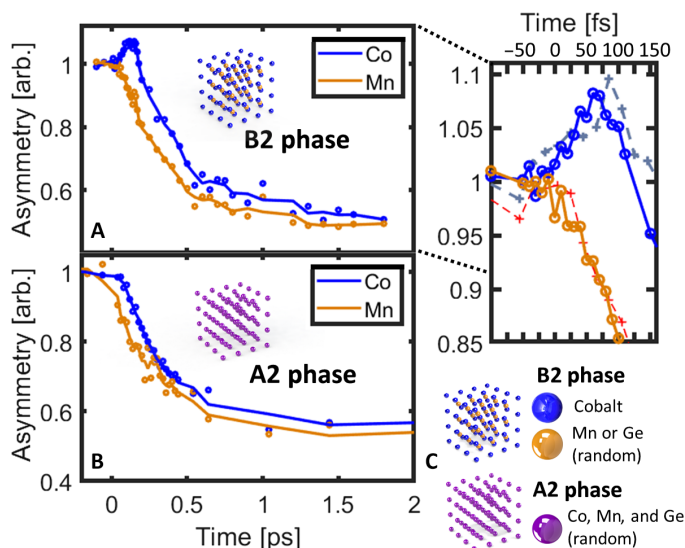


Fig. 2. Element-resolved ultrafast magnetization dynamics following excitation by a femtosecond laser. (A) In the half-metallic B2 phase, the Co magnetization increases as Mn decreases, with the changes happening as soon as light is incident on the material. Here, the open circles are the data points, and the solid lines represent a best fit to the data points. Inset: Dynamics of ultrafast spin transfer. Here, the lines link the actual data points. The blue and orange solid lines plot the magnetization of Mn and Co for a 55-fs (FWHM) pump pulse. The gray dashed lines show the broader response time for a longer 90-fs pump pulse. Note that the location of the peak of the enhancement is shifted in time by ~ 20 fs (approximately half the difference between the duration of the two pulses), underlining that this process is a direct optical manipulation. (B) Element-resolved ultrafast magnetization dynamics in the non-half-metallic A2 phase. There is no enhancement of the Co magnetization. (C) Atomic structure of the compounds studied. In the B2 phase, the Co atoms are ordered and occupy sites at the edges of the bcc structure, while the centers are randomly interspersed between Mn and Ge. In the A2 phase, the material has formed the ordered bcc structure, but the locations of atoms within the structure are random.

time delay. During the laser pulse, the Co magnetization transiently increases by $\approx 10\%$, while that of Mn immediately decreases. Although the initial dynamics are markedly different, the decay rates of the two magnetic sublattices are similar and occur on time scales similar to the average values measured by visible MOKE (2): Mn demagnetizes with an exponential decay constant of 328 ± 37 fs, while Co does so with a decay constant of 323 ± 86 fs (after a lag due to the initial transient enhancement). As the time scale for this process is longer than that in pure ferromagnets (see the Supplementary Materials), we can unambiguously decouple the direct optically generated spin dynamics (that occur over the entire laser pulse duration of 55 fs) from the dissipation of angular momentum in the system (that follows in the next picosecond). As yet another control to test the time sequence of spin transfer, we increased the pump pulse duration from 55 to 90 fs. As shown in dashed lines in the inset of Fig. 2A, this resulted in an increase of the delay in the demagnetization between the Co and Mn sublattices: from 120 ± 33 fs (55-fs pump pulse) to 157 ± 27 fs (90-fs pump pulse). This demonstrates that the ultrafast response is limited only by the duration of our pump pulse and is consistent with a spin transfer process from Mn to Co that occurs during the laser pump pulse.

Figure 2B plots the element-specific dynamics in the metallic A2 phase of the material. In this phase, the lag in response of the mag-

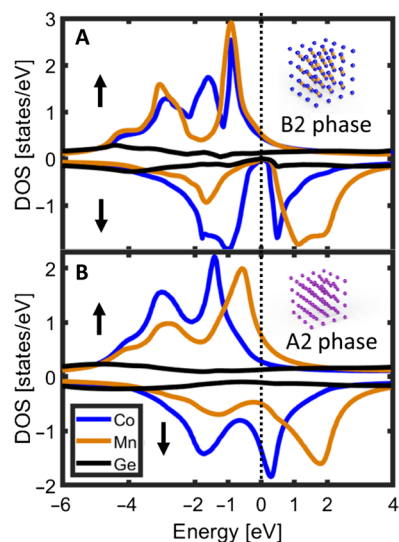


Fig. 3. Density of states for Co_2MnGe . Density of states (DOS) in the (A) B2 phase and (B) A2 phase. Note that the half-metallic character is only present in the B2 phase.

netic sublattices (Mn and Co) is much less, only 56 ± 32 fs, and no transient increase in the Co magnetization is observed. As discussed below and in the Supplementary Materials, this is because the optical pathways to excitation in the minority band of manganese are not blocked in this phase. Figure 2C shows the elemental crystal structure of the material in the two phases studied (B2 and A2). These measurements were taken on a separate sample [see the Supplementary Materials and (22) for further details on sample preparation]. Examining the density of states for Co_2MnGe (Fig. 3) shows that in contrast to the B2 phase, the A2 phase is disordered, does not have a half-metallic gap for the minority spin state (as shown in Fig. 3B), and serves as a control from which to understand the effect of half-metallicity on the element-specific magnetization properties of Co_2MnGe . The excitation pulse length for this measurement was 90 fs. Since the enhancement of the Co magnetization was observed with both 90- and 55-fs excitation pulses in the B2 phase, the use of a longer excitation pulse here does not affect our results.

It is clear from a comparison between the dynamics observed in the A2 and B2 phases that ordering and emergence of a half-metallic gap in the minority band play a fundamental role in the optical magnetic response of Co_2MnGe . The transient enhancement observed is a coherent process driven directly by the optical excitation pulse, as demonstrated by the shift in the peak of the Co excitation when driven by a longer laser pulse. Thus, our measurements also show that elemental specificity is critical for revealing the underlying magnetic dynamics of this material; i.e., as shown in Fig. 2 and the Supplementary Materials, if the Co and Mn responses were averaged (i.e., as done by visible MOKE measurements), no difference in the behavior of the A2 and B2 phases could be detected.

Figure 3 (A and B) plots the element-specific spin-resolved density of states calculated using DFT for the two phases of the material. In the B2 phase (Fig. 3A), a gap has formed for the minority carriers, while the majority has full mobility across the Fermi level. Critically, this gap is larger for the Mn states than for the Co states. In contrast, the crystal has a full metal characteristic in the A2 phase (Fig. 3B) for both the majority and minority states. When a 1.55-eV infrared photon is absorbed, the density of states of each phase results in several key

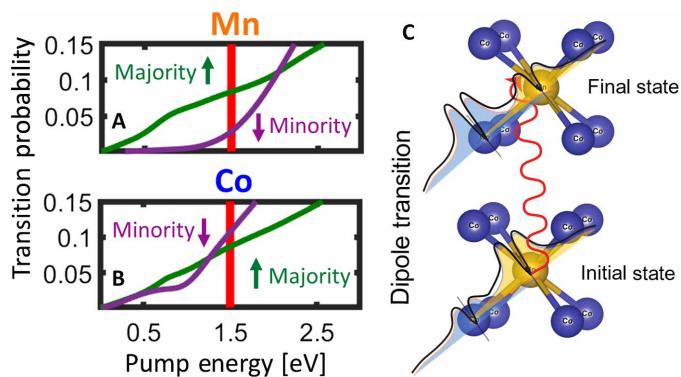


Fig. 4. Mechanism for direct light-induced spin transfer in Co_2MnGe . The probability for exciting a spin-up (majority) versus spin-down (minority) electron from the valence band in the B2 phase for different pump energies in (A) Mn sites. Note that for a 1.55-eV pump, the probability is higher for spin-up electrons to be excited from Mn. (B) Probability for excitations in Co sites. In contrast to the Mn result, the probability is higher for minority electrons to be excited in Co. (C) Illustration of a process that leads to direct optical transfer of spin polarization from Mn to Co. The initial-state wave function is hybridized and composed of both Mn and Co d-states, with a larger contribution from the Mn atom. In the final state, the situation is reversed, and the Co d-states dominate. Hence, when an electron is optically excited from the initial- to the final-state wave function, this is associated with a transfer of spin polarization from Mn to Co.

differences in the transition probabilities for the material. As shown in Fig. 4 and the Supplementary Materials, in the B2 phase, most of the minority carriers that are excited come from Co states, but very few minority excitations can take place for Mn states. One must bear in mind that both initial and final states of this optical excitation involve wave functions that are shared across hybridizing Mn and Co orbitals. Because of an imbalance in how Co and Mn projected orbitals contribute to the initial and final states, direct and spin-conserving transitions lead to an effective transfer of spin angular momentum from Mn to Co.

DISCUSSION

Figure 4 (A and B) plots the calculated imbalance of the transition probabilities from each sublattice that give rise to the spin transfer from Mn to Co. The combination of these effects results in a direct transfer of spin polarization from Mn sublattices to Co as observed experimentally in the B2 phase and illustrated in Fig. 1C. In Fig. 4C, we illustrate the basic mechanism that allows for an effective angular momentum transfer from Mn d-states to Co d-states. The initial-state wave function that is involved in the optical transition is hybridized and composed of both Mn and Co d-states, with a larger contribution from the Mn atom (initial state). For the final state, the situation is reversed, and the Co d-states dominate. Hence, when an electron is optically excited from the initial- to the final-state wave function, this is associated with a transfer of d-state population from Mn to Co. This is accomplished without any spin flip occurring, since spin is preserved in the optical excitation processes. A higher probability of transitions for the spin-up electrons compared to the spin-down electrons in Mn (Fig. 4A) then causes an effective spin transfer from Mn to Co, as observed in the data of Fig. 2A. In the A2 phase (Fig. 2B), excitation in the minority valence band of Mn is now optically allowed, no imbalance in the excitation probabilities exists, and direct optical transfer of spin polarization does not occur (see the Supplemen-

tary Materials for these calculations). As shown in Fig. 1C, the dominant light-induced pathway is primarily from the majority band in Mn, to shared conduction band wave functions that have a primarily Co character. This preserves the total spin but not the spin of the individual elements.

We emphasize that the transient enhancement of the magnetic signal shown in Fig. 2A for the B2 phase has no contribution from the change in refractive index due to electronic changes in the reflectivity. We demonstrate this by measuring the change in reflectivity for the B2 and A2 phases at the Co edge and showing that the magnitude of these changes is equal in the two phases of the material (see the Supplementary Materials for more information). The mechanism responsible for the magnetization dynamics of Co_2MnGe in the B2 phase involves direct optical transitions, leading to an initial transfer of spin moment from Mn to Co. This purely electronic mechanism is necessary in addition to a description based on the aLLG equation, which is sometimes employed to analyze the kind of experiments presented here (23, 24). As shown in the Supplementary Materials, the aLLG equation captures some features of the observed magnetization dynamics, especially at longer time scales (~ 250 fs and longer), but it fails to explain the initial phase of the demagnetization process. We also note that a similar enhancement to that shown in Fig. 2A was predicted via time-dependent DFT calculations for the related compound Co_2MnSi , with the mechanism in this case also attributed a transfer of spin polarization between Co and Mn (9).

Given that we now understand how to measure and predict all-optical spin transfer based on the electronic structure and the density of states of the material, future experiments can explore how changing the pump photon energy or tailoring the bandgap (i.e., density of states) (25) in other materials can be used to tune the demonstrated spin manipulation. Since the enhancement is only observed in the half-metallic phase of the material, the presence of the bandgap in the minority channel of both elements may help to enable the spin polarization enhancement in Co; after majority electrons are excited, they may not be able to decay via spin flip scattering into the minority band (8). We also note here that the B2 phase of Co_2MnGe , where the large spin transfer between two atom types is observed, is characterized by hybridizing states, as well as a low-spin state of one of the atoms (Co) that has a high-spin state available at not too large energies. Indeed, Co occupies this higher-spin state for the A2 phase. We speculate that these material characteristics are important when trying to find other materials that may have similar characteristics as those of Co_2MnGe and the results shown in Fig. 2A. The L2₁ phase shares these characteristics with the B2 phase of Co_2MnGe , and is therefore expected to have similar magnetization dynamics. There are several other materials that also have these characteristic properties. For instance, the meta-magnetic Laves phase YCo_2 , when doped with Fe or Ni, as well as fcc Fe doped with Co or Ni, are all systems that can be characterized in this way. Although direct spin transfer is likely the dominant mechanism in this material, we note that other sub-50-fs demagnetization mechanisms have recently been uncovered, and could cause different kinds of spin dynamics that operate on the same time scales as direct spin transfer in these other materials (16, 17). Finally, we note that a similar lag in spin dynamics was previously observed in alloys of FeNi (15); therefore, our element-resolved measurements of a lag in a fundamentally different system suggest that these phenomena may be ubiquitous.

Our time- and element-resolved EUV MOKE method will have useful applications for selecting spintronic materials, to understand

which materials are good candidates for spin injection. In the past several decades, various techniques for spin injection have emerged, but all have degrees of spin polarization <100%. Pursuing the goal of a pure spin current source, ferromagnetic half-metals were developed to ideally provide conduction of a single-spin state. However, 100% spin-polarized conduction has not yet been demonstrated in these compounds (26). Although many techniques are used to characterize the properties of half-metallic materials such as Andreev reflection (27, 28), spin-polarized tunneling, spin-polarized photoemission (29), and visible MOKE (3), these all rely on surface measurements. However, device applications require coherence and functionality through a finite nanoscale depth, and bulk and surface properties can be significantly different (30–34). A strong advantage of using EUV MOKE as a probe of these materials is the larger penetration depth of EUV light, more than twice that of visible light, which can, in addition to providing elemental specificity, probe the magnetization state of the material more deeply inside of a device. To use the potential of our findings in a functional spintronics device, the transfer of spin must occur across finite distances. According to DFT calculations, such a transfer process may be possible for a thin-film stack (14). Additionally, several new breakthroughs have recently reported miniaturizing spin current devices to the nanoscale (33, 34). Considering these recent developments, we anticipate that the femtosecond spin transfer demonstrated in this work could be used for information processing using spin currents on few-femtosecond time scales.

Within the context of spintronics, the ability to manipulate magnetization via the spatial transport of angular momentum has been the hallmark of many of the most important recent breakthroughs in the field. In the case of spin transfer torque, the discovery that one can transport angular momentum from one magnetic layer to another via spin-polarized current led to innovative new technology such as spin transfer torque magnetic random access memory. In the case of the spin Hall effect, the ability to efficiently transfer angular momentum between spatially remote interfaces with a pure spin current flowing in response to an applied electric field has opened the door to extremely fast spintronic devices. In this work, we spatially move angular momentum between neighboring atomic sites on the time scale of <10 fs. To put this in context, the equivalent 100% spin-polarized charge current required to generate such a massive torque in a spin transfer device is on the order of 10^{10} A/cm²—a current density that would instantaneously vaporize any metal! While the effect demonstrated here is transient in nature, it is not a fundamental limit of the physical process, but rather a limitation of the material system that we used. In principle, the transfer of angular momentum between atomic species could also affect the equilibrium magnetization in different materials.

In conclusion, we experimentally demonstrate the first direct optical manipulation of the magnetic moment of an individual element in a compound material. This ultrafast transfer is very likely a general feature of many materials, initiating as soon as light is incident on the material—near-instantaneously (femtosecond to attosecond time scales). A theory based on DFT as well as atomistic spin dynamics show that electronic excitations drive the magnetization dynamics in the initial phase of the demagnetization and that these excitations directly transfer spin from Mn to Co, via preferred spin-polarized excitation pathways. Rotation of atomic moments, as calculated by atomistic spin dynamics and that results in significant noncollinear orientations, becomes relevant at a later stage of the dynamics. We

confirm the predictions of the DFT calculations and importance of the half-metallic (B2) band structure of the material by a further lack of enhancement in the (A2) phase of the material (that lacks half-metallicity). This work represents the first optical manipulation of its kind and demonstrates a route to subfemtosecond all-optical logical operations in magnetic recording media.

MATERIALS AND METHODS

In this experiment, a Ti:Sapphire regenerative amplifier was used to generate 40-fs pulses of light with a center wavelength at 800 nm and a 40-nm (FWHM) bandwidth. The pulse energy directly from the amplifier was 2 mJ per pulse at a 5-kHz repetition rate, and 80% of this light (1.6 mJ) was used to generate the EUV light through high harmonic generation in a hollow core waveguide filled with helium gas. The EUV light was gently focused with a toroid, reflected from the sample at a 48° angle of incidence, and sent to a spectrometer. The spectrometer consists of a grating with 500 lines/mm that is mounted in a conical mount and an Andor charge-coupled device camera used in a full vertical binning mode. The pump pulse energy was 2.4 mJ/cm², and the spot size was measured via the knife edge method. Samples were dc magnetron sputter deposited at room temperature with the following thin-film structure: SiO₂/5-nm Ta/10-nm Co₂MnGe (CMG)/2.8-nm Ta. The CMG layer was formed by co-sputtering from a Co₂Mn target and the pure Ge target. The CMG was quasi-amorphous in the as-deposited state as confirmed by x-ray diffraction. The samples were ex situ annealed in high vacuum at or above 240°C to form a crystalline structure. Below 240°C, the structure remained quasi-amorphous with high resistivity and low magnetic moment.

SUPPLEMENTARY MATERIALS

Supplementary material for this article is available at <http://advances.sciencemag.org/cgi/content/full/6/3/eaaz1100/DC1>

Supplementary Text

Section S1. Further details of the experimental setup

Section S2. Sample preparation

Section S3. Change in reflectivity due to optical excitation in both phases

Section S4. Element-averaged response of the A2 and B2 phases

Section S5. Dynamics of Co₂MnGe on α -Al₂O₃

Section S6. Description of method for calculating the density of states and magnetic moment in Co₂MnGe

Section S7. Method for calculating the transition probabilities in Fig. 4

Section S8. Results of the calculations of *k*-conserving transition probabilities for the L21 phase

Section S9. Results of aLLG simulations

Fig. S1. Detailed experimental layout used to capture the element specific magnetic response of Co₂MnGe using EUV light.

Fig. S2. Static asymmetry measurements for the two phases of the material.

Fig. S3. Change in reflectivity measured for both the A2 and B2 phases.

Fig. S4. Total magnetization of sample plotted with element resolved signal.

Fig. S5. Element-resolved dynamics of Co₂MnGe (B2 phase) on sapphire.

Fig. S6. Element- and orbital-resolved density of states for the A2 and B2 phases.

Fig. S7. Transition probabilities for the dipole allowed transitions as a function of photon energy in the B2 phase of Co₂MnGe.

Fig. S8. Transition probabilities for the dipole-allowed transitions in the A2 phase.

Fig. S9. Transition probabilities for Mn and Co in the A2 phase.

Fig. S10. *k*-conserving transition probabilities for the L21 phase compared to non *k*-conserving transitions.

Fig. S11. Element-resolved demagnetization in Co₂MnGe for the L2₁, A2, and B2 phases.

Table S1. Fitting parameters of the double exponential function to fit *M*(*t*)/*M*(0).

Table S2. Site-resolved Gilbert damping parameter in the L2₁ phase.

Table S3. Site-resolved Gilbert damping parameter in the A2 phase.

Table S4. Site-resolved Gilbert damping parameter in the B2 phase.

Table S5. Fitting parameters for fits performed to the functions used in the main text.

References (35–42)

REFERENCES AND NOTES

- G. A. Prinz, Spin-polarized transport. *Phys. Today* **48**, 58–63 (1995).
- A. Mann, J. Walowski, M. Münzenberg, S. Maat, M. J. Carey, J. R. Childress, C. Mewes, D. Ebke, V. Drewello, G. Reiss, A. Thomas, Insights into ultrafast demagnetization in pseudogap half-metals. *Phys. Rev. X* **2**, 041008 (2012).
- G. M. Müller, J. Walowski, M. Djordjevic, G.-X. Miao, A. Gupta, A. V. Ramos, K. Gehrke, V. Moshnyaga, K. Samwer, J. Schmalhorst, A. Thomas, A. Hütten, G. Reiss, J. S. Moodera, M. Münzenberg, Spin polarization in half-metals probed by femtosecond spin excitation. *Nat. Mater.* **8**, 56–61 (2009).
- S. He, Y. Liu, Y. Zheng, Q. Qin, Z. Wen, Q. Wu, Y. Yang, Y. Wang, Y. P. Feng, K. L. Teo, C. Panagopoulos, Tunable magnetization relaxation of $\text{Fe}_2\text{Cr}_{1-x}\text{Co}_x\text{Si}$ half-metallic Heusler alloys by band structure engineering. *Phys. Rev. Mater.* **1**, 064401 (2017).
- E. Beaurepaire, J.-C. Merle, A. Daunois, J.-Y. Bigot, Ultrafast spin dynamics in ferromagnetic nickel. *Phys. Rev. Lett.* **76**, 4250 (1996).
- A. Scholl, L. Baumgarten, R. Jacquemin, W. Eberhardt, Ultrafast spin dynamics of ferromagnetic thin films observed by fs spin-resolved two-photon photoemission. *Phys. Rev. Lett.* **79**, 5146 (1997).
- T. Li, A. Patz, L. Mouchliadis, J. Yan, T. A. Lograsso, I. E. Perakis, J. Wang, Femtosecond switching of magnetism via strongly correlated spin-charge quantum excitations. *Nature* **496**, 69–73 (2013).
- A. J. Schellekens, K. C. Kuiper, R. R. J. C. de Wit, B. Koopmans, Ultrafast spin-transfer torque driven by femtosecond pulsed-laser excitation. *Nat. Commun.* **5**, 4333 (2014).
- C.-H. Lambert, S. Mangin, B. S. D. C. S. Varapasad, Y. K. Takahashi, M. Hehn, M. Cinchetti, G. Malinowski, K. Hono, Y. Fainman, M. Aeschlimann, E. E. Fullerton, All-optical control of ferromagnetic thin films and nanostructures. *Science* **345**, 1337–1340 (2014).
- S. Mangin, M. Gottwald, C.-H. Lambert, D. Steil, V. Uhlir, L. Pang, M. Hehn, S. Alebrand, M. Cinchetti, G. Malinowski, Y. Fainman, M. Aeschlimann, E. E. Fullerton, Engineered materials for all-optical helicity-dependent magnetic switching. *Nat. Mater.* **13**, 286–292 (2014).
- D. Steil, S. Alebrand, T. Roth, M. Krauß, T. Kubota, M. Oogane, Y. Ando, H. C. Schneider, M. Aeschlimann, M. Cinchetti, Band-structure-dependent demagnetization in the Heusler alloy $\text{Co}_2\text{Mn}_{1-x}\text{Fe}_x\text{Si}$. *Phys. Rev. Lett.* **105**, 17–20 (2010).
- J.-P. Wüstenberg, D. Steil, S. Alebrand, T. Roth, M. Aeschlimann, M. Cinchetti, Ultrafast magnetization dynamics in the half-metallic Heusler alloy $\text{Co}_2\text{Cr}_{0.6}\text{Fe}_{0.4}\text{Al}$. *Phys. Status Solidi Basic Res.* **248**, 2330–2337 (2011).
- P. Elliott, T. Müller, J. K. Dewhurst, S. Sharma, E. K. U. Gross, Ultrafast laser induced local magnetization dynamics in Heusler compounds. *Sci. Rep.* **6**, 38911 (2016).
- J. Dewhurst, P. Elliott, S. Shallcross, E. K. U. Gross, S. Sharma, Laser induced inter-site spin transfer. *Nano Lett.* **18**, 1842–1848 (2018).
- S. Mathias, C. la-O-Vorakiat, P. Grychtol, P. Granitzka, E. Turgut, J. M. Shaw, R. Adam, H. T. Nembach, M. E. Siemens, S. Eich, C. M. Schneider, T. J. Silva, M. Aeschlimann, M. M. Murnane, H. C. Kapteyn, Probing the timescale of the exchange interaction in a ferromagnetic alloy. *Proc. Natl. Acad. Sci. U.S.A.* **109**, 4792–4797 (2012).
- P. Tengdin, W. You, C. Chen, X. Shi, D. Zusin, Y. Zhang, C. Gentry, A. Blonsky, M. Keller, P. M. Oppeneer, H. C. Kapteyn, Z. Tao, M. M. Murnane, Critical behavior within 20 fs drives the out-of-equilibrium laser-induced magnetic phase transition in nickel. *Sci. Adv.* **4**, eaap9744 (2018).
- R. Gort, K. Bühlmann, S. Däster, G. Salvatella, N. Hartmann, Y. Zemp, S. Holenstein, C. Stieger, A. Fognini, T. U. Michlmayr, T. Bähler, A. Vaterlaus, Y. Acremann, Early stages of ultrafast spin dynamics in a 3d ferromagnet. *Phys. Rev. Lett.* **121**, 087206 (2018).
- P. Hohenberg, W. Kohn, The inhomogeneous electron gas. *Phys. Rev.* **136**, B864–B871 (1964).
- W. Kohn, L. J. Sham, Self-consistent equations including exchange and correlation effects. *Phys. Rev.* **140**, A1133–A1138 (1965).
- O. Eriksson, A. Berman, L. Bergqvist, J. Hellsvik, *Atomistic Spin Dynamics: Foundations and Applications* (Oxford Univ. Press, 2017).
- C. La-O-Vorakiat, M. Siemens, M. M. Murnane, H. C. Kapteyn, S. Mathias, M. Aeschlimann, P. Grychtol, R. Adam, C. M. Schneider, J. M. Shaw, H. Nembach, T. J. Silva, Ultrafast demagnetization dynamics at the M edges of magnetic elements observed using a tabletop high-harmonic soft X-ray source. *Phys. Rev. Lett.* **103**, 257402 (2009).
- J. M. Shaw, E. K. Delczeg-Czirjak, E. R. J. Edwards, Y. Kvashnin, D. Thonig, M. A. W. Schoen, M. Pufall, M. L. Schneider, T. J. Silva, O. Karis, K. P. Rice, O. Eriksson, H. T. Nembach, Magnetic damping in sputter-deposited Co_2MnGe Heusler compounds with A2, B2, and L2₁ orders: Experiment and theory. *Phys. Rev. B* **97**, 094420 (2018).
- R. F. L. Evans, U. Atxitia, R. W. Chantrell, Quantitative simulation of temperature-dependent magnetization dynamics and equilibrium properties of elemental ferromagnets. *Phys. Rev. B* **91**, 144425 (2015).
- M. Hofherr, S. Moretti, J. Shim, S. Häuser, N. Y. Safonova, M. Stiehl, A. Ali, S. Sakshath, J. W. Kim, D. H. Kim, H. J. Kim, J. I. Hong, H. C. Kapteyn, M. M. Murnane, M. Cinchetti, D. Steil, S. Mathias, B. Stadtmüller, M. Albrecht, D. E. Kim, U. Nowak, M. Aeschlimann, Induced versus intrinsic magnetic moments in ultrafast magnetization dynamics. *Phys. Rev. B* **98**, 174419 (2018).
- P. Klaer, M. Kallmayer, C. G. F. Blum, T. Graf, J. Barth, B. Balke, G. H. Fecher, C. Felser, H. J. Elmers, Tailoring the electronic structure of half-metallic Heusler alloys. *Phys. Rev. B* **80**, 144405 (2009).
- X. Y. Dong, C. Adelman, J. Q. Xie, C. J. Palmström, X. Lou, J. Strand, P. A. Crowell, J. P. Barnes, A. K. Petford-Long, Spin injection from the Heusler alloy Co_2MnGe into $\text{Al}_0.1\text{Ga}_{0.9}\text{As}/\text{GaAs}$ heterostructures. *Appl. Phys. Lett.* **86**, 102107 (2005).
- A. F. Andreev, The thermal conductivity of the intermediate state in superconductors. *J. Exp. Theor. Phys.* **19**, 1228–1231 (1964).
- J. N. Kupferschmidt, P. W. Brouwer, Andreev reflection at half-metal/superconductor interfaces with nonuniform magnetization. *Phys. Rev. B* **83**, 014512 (2011).
- Z. Sun, Q. Wang, J. F. Douglas, H. Lin, S. Sahrakorpi, B. Barbiellini, R. S. Markiewicz, A. Bansil, A. V. Fedorov, E. Rotenberg, H. Zheng, J. F. Mitchell, D. S. Dessau, Minority-spin t_{2g} states and the degree of spin polarization in ferromagnetic metallic $\text{La}_{2-2x}\text{Sr}_{1+2x}\text{Mn}_2\text{O}_7$ ($x = 0.38$). *Sci. Rep.* **3**, 3167 (2013).
- J. J. Attema, L. Chioncel, C. M. Fang, G. A. de Wijs, R. A. de Groot, Half-metals: Challenges in spintronics and routes toward solutions. *Lect. Notes Phys.* **678**, 199–216 (2005).
- M. E. Fisher, The theory of equilibrium critical phenomena. *Rep. Prog. Phys.* **30**, 615–730 (1967).
- T. Pincelli, V. Lollobrigida, F. Borgatti, A. Regoutz, B. Gobaut, C. Schlueter, T.-L. Lee, D. J. Payne, M. Oura, K. Tamasaku, A. Y. Petrov, P. Graziosi, F. M. Granozio, M. Cavallini, G. Vinai, R. Ciprian, C. H. Back, G. Rossi, M. Taguchi, H. Daimon, G. van der Laan, G. Panaccione, Quantifying the critical thickness of electron hybridization in spintronic materials. *Nat. Commun.* **8**, 16051 (2017).
- K. Wagner, A. Kákay, K. Schultheiss, A. Henschke, T. Sebastian, H. Schultheiss, Magnetic domain walls as reconfigurable spin-wave nanochannels. *Nat. Nanotechnol.* **11**, 432–436 (2016).
- V. V. Kruglyak, S. O. Demokritov, D. Grundler, Magnonics. *J. Phys. D: Appl. Phys.* **43**, 264001 (2010).
- H. Ebert, D. Ködderitzsch, J. Minár, Calculating condensed matter properties using the KKR-Green's function method—Recent developments and applications. *Rep. Prog. Phys.* **74**, 096501 (2011).
- P. Soven, Coherent-potential model of substitutional disordered alloys. *Phys. Rev.* **156**, 809–813 (1967).
- G. M. Stocks, W. M. Temmerman, B. L. Gyorffy, Complete solution of the Korringa-Kohn-Rostoker coherent-potential-approximation equations: Cu-Ni alloys. *Phys. Rev. Lett.* **41**, 339–343 (1978).
- S. H. Vosko, L. W. M. Nussair, Accurate spin-dependent electron liquid correlation energies for local spin density calculations: A critical analysis. *Can. J. Phys.* **58**, 1200–1211 (1980).
- V. Antropov, M. Katsnelson, B. Harmon, M. van Schilfgaarde, Spin dynamics in magnets: Equation of motion and finite temperature effects. *Phys. Rev. B* **54**, 1019–1035 (1996).
- B. Skubic, J. Hellsvik, L. Nordström, O. Eriksson, A method for atomistic spin dynamics simulations: Implementation and examples. *J. Phys. Condens. Matter* **20**, 315203 (2008).
- J. H. Mentink, J. Hellsvik, D. V. Afanasiev, B. A. Ivanov, A. Kirilyuk, A. V. Kimel, O. Eriksson, M. I. Katsnelson, T. Rasing, Ultrafast spin dynamics in multisublattice magnets. *Phys. Rev. Lett.* **108**, 57202 (2012).
- G. Malinowski, F. Dalla Longa, J. H. H. Rietjens, P. V. Paluskar, R. Huijink, H. J. M. Swagten, B. Koopmans, Control of speed and efficiency of ultrafast demagnetization by direct transfer of spin angular momentum. *Nat. Phys.* **4**, 855–858 (2008).

Acknowledgments: We thank B. Stadtmüller, P. Oppeneer, J. Ellis, L. Mijaja-Avila, K. Dorney, Q. Nguyen, N. Brooks, D. Morrill, and A.N. Yaresko for helpful discussions. **Funding:** The experimental measurements were performed at JILA. M.M.M. and H.C.K. acknowledge support for the measurements from the Department of Energy Office of Basic Energy Sciences X-Ray Scattering Program Award DE-SC0002002 for the X-ray spectroscopy, the DARPA TEE Award no. D18AC00017 for the HHG source, and the Gordon and Betty Moore Foundation EPIQS Award GBMF4538. J.S., M.A., H.N., and T.J.S. acknowledge support from a DOE grant (DE-SC0017643). Y.K., E.K.D.-C., and O.E. acknowledge the Swedish National Infrastructure for Computing (SNIC) for computational resources and the Swedish Foundation for Strategic Research (SSF), the Swedish Research Council (VR), STandUP, eSSENCE, and the Knut and Alice Wallenberg Foundation (KAW) for financial support. **Author contributions:** M.M.M., H.C.K., S.M., J.S., and P.T. conceived the project. P.T., C.G., A.B., D.Z., M.G., and L.H. conducted the experiments. P.T. and C.G. analyzed the data. J.S.,

M.Ar., H.N., and T.J.S. prepared the samples. Y.K., E.K.D.-C., and O.E. performed and analyzed DFT calculations. K.K., D.T., and O.E. performed and analyzed the aLLG simulations. P.T., M.M., C.G., A.B., D.Z., H.K., Y.K., O.E., E.D.-Z., S.M., M.H., and M.Ae. discussed and evaluated experimental results. P.T., C.G., and M.M.M. wrote the manuscript with inputs from all other authors. **Competing interests:** H.C.K. and M.M.M. have a financial interest in KMLabs, which produced the lasers and high harmonic generation sources used in this work. H.C.K. is partially employed by KMLabs. The authors declare that they have no other competing interests. **Data and materials availability:** All data needed to evaluate the conclusions in the paper are present in the paper and/or the Supplementary Materials. Additional data related to this paper may be requested from the authors.

Submitted 12 December 2018

Accepted 26 November 2019

Published 17 January 2020

10.1126/sciadv.aaz1100

Citation: P. Tengdin, C. Gentry, A. Blonsky, D. Zusin, M. Gerrity, L. Hellbrück, M. Hofherr, J. Shaw, Y. Kvashnin, E. K. Delczeg-Czirjak, M. Arora, H. Nembach, T. J. Silva, S. Mathias, M. Aeschlimann, H. C. Kapteyn, D. Thonig, K. Koumpouras, O. Eriksson, M. M. Murnane, Direct light-induced spin transfer between different elements in a spintronic Heusler material via femtosecond laser excitation. *Sci. Adv.* **6**, eaaz1100 (2020).

Direct light–induced spin transfer between different elements in a spintronic Heusler material via femtosecond laser excitation

Phoebe Tengdin, Christian Gentry, Adam Blonsky, Dmitriy Zusin, Michael Gerrity, Lukas Hellbrück, Moritz Hofherr, Justin Shaw, Yaroslav Kvashnin, Erna K. Delczeg-Czirjak, Monika Arora, Hans Nembach, Tom J. Silva, Stefan Mathias, Martin Aeschlimann, Henry C. Kapteyn, Danny Thonig, Konstantinos Koumpouras, Olle Eriksson and Margaret M. Murnane

Sci Adv **6** (3), eaaz1100.
DOI: 10.1126/sciadv.aaz1100

ARTICLE TOOLS

<http://advances.sciencemag.org/content/6/3/eaaz1100>

SUPPLEMENTARY MATERIALS

<http://advances.sciencemag.org/content/suppl/2020/01/13/6.3.eaaz1100.DC1>

REFERENCES

This article cites 41 articles, 3 of which you can access for free
<http://advances.sciencemag.org/content/6/3/eaaz1100#BIBL>

PERMISSIONS

<http://www.sciencemag.org/help/reprints-and-permissions>

Use of this article is subject to the [Terms of Service](#)

Science Advances (ISSN 2375-2548) is published by the American Association for the Advancement of Science, 1200 New York Avenue NW, Washington, DC 20005. The title *Science Advances* is a registered trademark of AAAS.

Copyright © 2020 The Authors, some rights reserved; exclusive licensee American Association for the Advancement of Science. No claim to original U.S. Government Works. Distributed under a Creative Commons Attribution NonCommercial License 4.0 (CC BY-NC).